C. R. Physique 15 (2014) 318–328

Contents lists available at ScienceDirect

Comptes Rendus Physique

www.sciencedirect.com

Ultra-high-energy cosmic rays / Rayons cosmiques d'ultra-haute énergie

Cosmic rays from the ankle to the cutoff

Les rayons cosmiques, de la cheville à la coupure

Karl-Heinz Kampert [a,*], Peter Tinyakov [b,*]

[a] *University Wuppertal, Department of Physics, 42119 Wuppertal, Germany*
[b] *Service de physique théorique, Université libre de Bruxelles, CP225, boulevard du Triomphe, B-1050 Brussels, Belgium*

ARTICLE INFO

Article history:
Available online 3 May 2014

Keywords:
UHECR
Energy spectrum
Mass composition
Anisotropy

Mots-clés :
Rayons cosmiques
Composition masse
Anisotropie

ABSTRACT

Recent advances in measuring and interpreting cosmic rays from the spectral ankle to the highest energies are briefly reviewed. The prime question at the highest energies is about the origin of the flux suppression observed at $E \simeq 4 \cdot 10^{19}$ eV. Is this the long-awaited GZK-effect or the exhaustion of sources? The key to answering this question will be provided by the largely unknown mass composition at the highest energies. The high level of isotropy observed even at the highest energies challenges models of a proton-dominated composition if extragalactic magnetic fields are on the order of a few nG or less. We shall discuss the experimental and theoretical progress in the field and the prospects for the next decade.

© 2014 Académie des sciences. Published by Elsevier Masson SAS. All rights reserved.

RÉSUMÉ

Les récentes avancées des mesures et de l'interprétation des rayons cosmiques, depuis la caractéristique spectrale appelé « cheville » jusqu'aux plus hautes énergies, sont brièvement revues. Aux plus hautes énergie, la question principale concerne l'origine de la suppression du flux observée au dessus de $4 \cdot 10^{19}$ eV. Est-ce la prédiction GZK tant attendue, ou bien l'épuisement des sources ? La réponse à cette question sera fournie par la mesure de la composition des rayons cosmiques aux plus hautes énergies, qui est aujourd'hui largement inconnue. L'isotropie des directions d'arrivée observées même aux plus hautes énergies défavorise les modèles où les protons dominent la composition, si les champs magnétiques extragalactiques sont au plus de quelques nG. Nous discuterons les progrès expérimentaux et théoriques du domaine et les perspectives pour la prochaine décennie.

© 2014 Académie des sciences. Published by Elsevier Masson SAS. All rights reserved.

1. Introduction

In the last decade, a new generation of the ultra-high energy cosmic ray (UHECR) observatories has come into operation: the Pierre Auger Observatory in the Southern Hemisphere and the Telescope Array in the Northern one. Apart from a

* Corresponding authors.
E-mail addresses: kampert@uni-wuppertal.de (K.-H. Kampert), petr.tiniakov@ulb.ac.be (P. Tinyakov).

http://dx.doi.org/10.1016/j.crhy.2014.04.006
1631-0705/© 2014 Académie des sciences. Published by Elsevier Masson SAS. All rights reserved.

significant advance in size over their predecessors, both observatories have implemented, for the first time, a new hybrid technique of the UHECR detection where the same air shower is observed simultaneously by a ground array of particle detectors and by fluorescence telescopes capable of tracing the development of the air shower in the atmosphere. By now, both observatories have accumulated a significant part of their lifetime statistics. It may be time, therefore, to summarize the advances in our understanding of UHECR and formulate the remaining problems.

The Pierre Auger Observatory (Auger) [1] is located in Argentina (centered at 69°20 W, 35°20 S) at 1400 m above sea level, corresponding to 870 g/cm^2. It consists of a Surface Detector array (SD) comprising 1660 autonomously operated water-Cherenkov detectors of 10 m^2 area each. The tanks are filled with 12 tons of purified water and three photomultipliers are used to detect the Cherenkov light produced by charged particles. The surface detectors are spread over a 3000 km^2 area and are placed on a triangular grid of 1.5-km spacing. The SD array is overlooked by 27 fluorescence detector telescopes (FD) distributed at five sites [2]. Stable data taking started in January 2004 and the Observatory has been running with its full configuration since 2008.

The Telescope Array (TA) is located in Utah, USA, at 39°30 N, 112°91 W at an altitude of about 1400 m above sea level. It consists of 507 plastic scintillator detectors of 3-m^2 area each spread over approximately 700 km^2 (for details see [3]). The detectors are placed on a square grid with a spacing of 1.2 km. The atmosphere over the surface array is viewed by 38 fluorescence telescopes arranged in three stations [4]. TA is fully operational since March 2008.

Despite similar hybrid design, the two experiments have a number of differences that should be kept in mind when comparing the results. The main one is the design of the ground array detectors. The detectors of TA are traditional two layers of 1.2-cm-thick plastic scintillators, similar to the single 5-cm-thick layers used in AGASA. The water tanks of the Pierre Auger Observatory have a thickness of 1.2 m and a large overall volume, which makes them more sensitive than the TA detectors, especially to inclined particles. At the same time, the large thickness enhances the signal due to the penetrating muonic component of a shower, which is more difficult to model.

By now, an unprecedented number of UHECR events have been detected by the ground arrays and the fluorescent telescopes of both experiments. At energies $E > 10^{19}$ eV, over 10^4 events have been recorded by the Pierre Auger Observatory, and over 2×10^3 by the Telescope Array. For each event, several observables can be reconstructed, the key ones being the energy of the primary particle, the arrival direction and, for the events detected by the fluorescence telescopes, the atmospheric depth of the air shower maximum. These and other observables allow one to shed some light on the nature of primary particles and the origins of UHECR, as discussed in the next sections.

2. Energy spectra

The all-particle energy spectrum is perhaps the most prominent observable of cosmic rays being investigated. It carries combined information about the UHECR sources and about the Galactic and/or intergalactic media in which CRs propagate. The ankle, a hardening seen in the all-particle spectrum at about $5 \cdot 10^{18}$ eV, is generally considered to mark the transition from Galactic to extragalactic cosmic rays. However, recent measurements of KASCADE-Grande [5,6] suggest that this transition may occur more than an order of magnitude lower in energy, i.e. around 10^{17} eV. At this energy, the component of light elements is subdominant, but exhibits a hardening to become dominant at the ankle. The so-called dip-model of the ankle [7] interprets the ankle as being the imprint of protons suffering e^+e^- pair-production in the CMB. Thus, it requires protons to be dominant at energies significantly above and below the ankle and the transition to occur again below the ankle energy. Obviously, models differ in their energy spectra expected for different mass groups and thereby in their cosmic ray mass composition as a function of energy. Related to this, one also expects to see different levels of anisotropies in the arrival directions, as it will be difficult to fully isotropize EeV protons in Galactic magnetic fields [8].

At the highest energy, a flux suppression due to energy losses by photo-pion production and photo-disintegration in the CMB is expected for protons and nuclei, respectively. In fact, this so-called GZK-effect [9,10] is the only firm prediction ever made concerning the shape of the UHECR spectrum. First observations of a cutoff were reported by HiRes and Auger [11,12]. However, at present we cannot be sure whether this flux suppression is an imprint of the aforementioned GZK energy losses or whether it is related to the maximum cosmic ray acceleration energy at the sources.

A first comprehensive comparison of available data was performed by a joint working group of Auger, TA, HiRes, and Yakutsk and is presented in [13]. It is found that the energy spectra determined by the Auger and TA observatories are consistent in normalization and shape if the uncertainties in the energy scale – at that time quoted for each experiment to be about 20% – are taken into account. This is a quite notable achievement and it demonstrates how well the data of current observatories are understood.

The most recent updates of the cosmic-ray energy spectra were presented at the ICRC 2013 Conference. Auger has reported an exposure of about 40 000 km^2 sr yr in the zenith angle range up to 80°. TA, due to its later start and its more than four times smaller area, has collected about a 10th of the events. The TA collaboration restricts the analysis to zenith angles below 45°, which can be understood from the smaller vertical dimensions of the scintillator slabs compared to the 1.2-m height of the water tanks. Taking into account recent precise measurements of the fluorescence yield [17] and taking advantage of a better estimate of the invisible energy, a deeper understanding of the detector and consequently improved event reconstruction, the Pierre Auger Collaboration has recently updated their cosmic-ray energy scale and reduced its systematic uncertainties to 14% [18]. The corresponding results of the two experiments are presented in Fig. 1. The energy

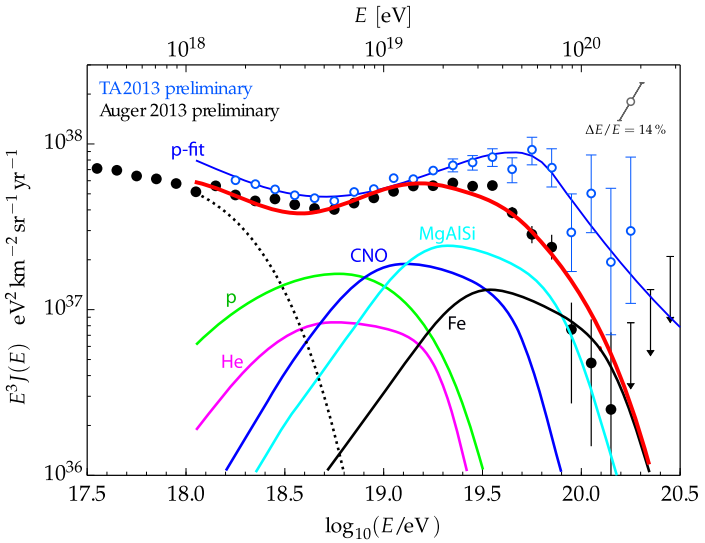

Fig. 1. Recent measurements of the flux of CRs at the highest energies by the Auger and TA collaborations [14,15]. The TA-data are fitted to a model of extragalactic proton sources, distributed cosmologically according to $(1+z)^{4.4}$ and injecting a power-law distribution at the sources according to $E^{-2.39}$ (blue line). The Auger data are compared to a model assuming a maximum acceleration energy $E_{\max} = 10^{18.7}$ eV $\times Z$ with injection spectra $\gamma = 1$ and an enhanced Galactic cosmic ray composition from [16]. An additional Galactic component is plotted as a dotted black line. (For interpretation of the references to color in this figure, the reader is referred to the web version of this article.)

spectra of the two observatories clearly exhibit the ankle at $\sim 5 \cdot 10^{18}$ eV and a flux suppression above $\sim 4 \cdot 10^{19}$ eV, and are compared to simplified astrophysical scenarios with parameters given in the figure caption.

As can be seen from this comparison, the ankle occurs at an energy which is compatible with the dip-model under the assumption of a pure proton composition. Also, the flux suppression at the highest energies is in accordance with the energy loss processes of the GZK-effect. In the case of Auger, however, the suppression starts at lower energies as compared to the propagation calculations unless the maximum energy of sources is set to approximately 10^{20} eV [15]. It is important to realize that the suppression region of the spectrum can also be described by assuming pure Fe-emission from the sources. In this case, however, the ankle would require another component of cosmic rays to contribute to the flux at lower energies. Another interpretation of the suppression region has been presented in, e.g., [19–22]. In this group of models, the flux suppression is primarily caused by the limiting acceleration energy at the sources rather than by the GZK-effect. A good description of the Auger all-particle energy spectrum is obtained for $E_{\max,\mathrm{p}} \simeq 10^{18.7}$ eV, with a mix of protons and heavier nuclei being accelerated up to the same rigidity, so that their maximum energy scales like $E_{\max,Z} \propto Z \times E_{\max,\mathrm{p}}$ (colored histograms in Fig. 1 [16]). Obviously, the latter class of models (which also account for all relevant energy loss processes during propagation [23]) leads to an increasingly heavier composition towards the suppression region. We shall return to this aspect in the next section. Another notable feature of such classes of models is the requirement of injection spectra considerably harder than those expected from Fermi acceleration. This was pointed out also, e.g., in Refs. [22,16,24]. However, as recently discussed in [25], the effects of diffusion of high-energy cosmic rays in turbulent extragalactic magnetic fields counteract the requirement of hard injection spectra ($\gamma < 2.0$) for a reasonable range of magnetic field strengths and coherence lengths.

The different interpretations of the Auger and TA energy spectra demonstrate the ambiguity left by the all-particle energy spectrum and they underline the importance of understanding the absolute cosmic-ray energy scales to a high level of precision. While perfect agreement is seen up to the ankle and beyond, one finds that the flux suppression in the Auger data not only starts at somewhat lower energies, but also falls off more strongly than in TA data. This difference – despite being still compatible with the quoted systematic uncertainties of TA and Auger of 20% and 14% – deserves further attention.

3. Mass composition

Obviously the all-particle energy spectrum by itself, despite the high level of precision reached, does not allow one to conclude about the origin of the spectral structures and thereby about the origin of cosmic rays from the ankle to the highest energies. Additional key information is obtained from the mass composition of cosmic rays. Unfortunately, the measurement of primary masses is the most difficult task in air-shower physics as it relies on comparisons of data to EAS simulations with the latter serving as reference [26,27]. EAS simulations, however, are subject to uncertainties mostly because hadronic interaction models need to be employed at energy ranges much beyond those accessible to man-made particle accelerators. Therefore, the advent of LHC data, particularly those measured in the extreme forward region of the collisions, is of great importance to cosmic ray and air shower physics and has been awaited with great interest [26]. Remarkably, interaction models employed in air shower simulations provided a somewhat better prediction of global observables (multiplicities,

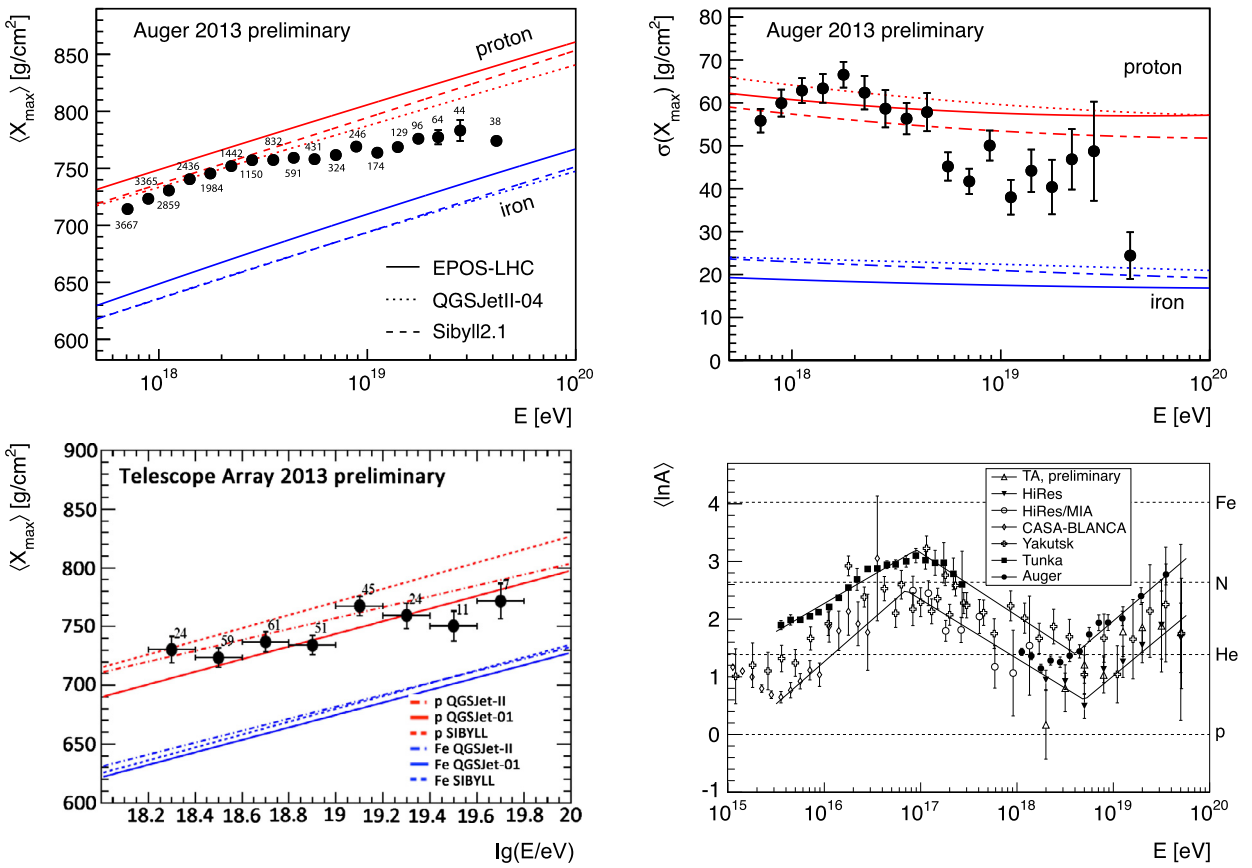

Fig. 2. Top: Evolution of $\langle X_{\max}\rangle$ and $\sigma(X_{\max})$ with energy in data from the Pierre Auger Observatory [15]. Bottom left: $\langle X_{\max}\rangle$ as a function of energy from TA [30]. Bottom right: Average logarithmic mass of CRs as a function of energy derived from $X_{\max}$ measurements with optical detectors for the EPOS 1.99 interaction model. Lines are estimates of the experimental systematics, i.e. upper and lower boundaries of the data presented [26].

$p_\perp$-distributions, forward and transverse energy flow, etc.) than typical tunes of HEP models, such as PYTHIA or PHOJET [28]. This revealed that the cosmic-ray community has taken great care in extrapolating models to the highest energies. Moreover, as demonstrated, e.g., in [29], cosmic-ray data provide important information about particle physics at center-of-mass energies ten or more times higher than is accessible at LHC. The pp inelastic cross section extracted from data of the Pierre Auger Observatory supports only a modest rise of the inelastic pp cross section with energy [29].

A careful analysis of composition data from various experiments has been performed and reviewed in [26,31]. Updated results from the TA and Auger Observatories as well as a comparison of the two were presented at the ICRC 2013 with exemplary results depicted in Fig. 2. The data from the Pierre Auger Observatory (Fig. 2, top panel) suggest an increasingly heavy mass composition above $4 \cdot 10^{18}$ eV when compared to post-LHC interaction models. The TA data are compatible with a proton-dominated composition at all energies (Fig. 2, bottom left) but have much larger statistical uncertainties and are compared to pre-LHC interaction models which showed a larger scatter and mostly predicted shallower showers. It is important to note that the datapoints and model predictions of TA and Auger cannot be compared directly to each other. This is because TA applies detector specific acceptance cuts to data and Monte Carlo simulations, while Auger applies fiducial volume cuts aimed at selecting a bias-free event sample. This is done by using a high-quality hybrid data set and applying fiducial volume cuts based on the shower geometry that ensure that the viewable $X_{\max}$ range for each shower is large enough to accommodate the full $X_{\max}$ distribution [32]. The price to be paid for these so-called anti-bias cuts enabling a direct data-to-model comparison is that it requires significantly more statistics than the classical method of applying the same cuts to models and data. Because of this, it is presently not yet available in the TA data. The event statistics surviving all cuts and entering the $X_{\max}$ energy bins of the Auger and TA data sample is specified in Fig. 2. Because of these complications, both collaborations have started to jointly investigate the origin of these differences in $X_{\max}$ by injecting the measured composition from the Pierre Auger Observatory into the TA Monte Carlo. The result of that preliminary study shows that the proton- and Auger-like composition cannot be discriminated from one another within the presently available TA statistics [33]. It will be interesting to see this puzzle being solved in the near future both by refined and improved reconstruction and analysis techniques, as well as by collecting more data.

A (pre-ICRC 2013) compilation of composition data from various experiments is depicted in Fig. 2 (bottom right). These data complement those of the energy spectrum in a remarkable way. As can be seen, the breaks in the energy spectrum

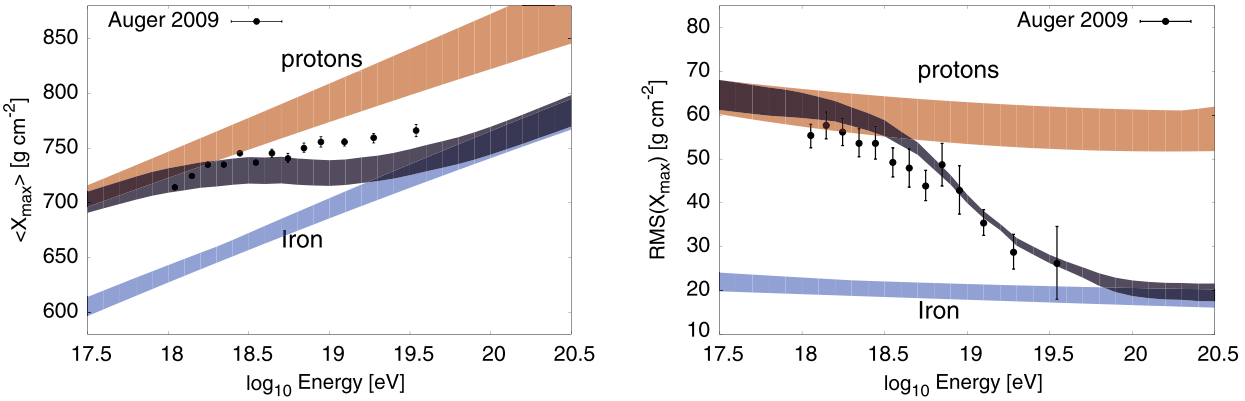

Fig. 3. Example of $\langle X_{\max}\rangle$ and RMS($X_{\max}$) predicted by the archetypal maximum energy model of [22] in comparison to data from the Auger observatory.

coincide with the turning points of changes in the composition: the mean mass becomes increasingly heavier above the knee, reaches a maximum near the 'iron-knee', another minimum at the ankle, before it starts to modestly rise again towards the highest energies. Different interaction models provide the same answer concerning changes in the composition, but differ by their absolute values of $\langle \ln A\rangle$ [26,34].

The interpretation of the all-particle energy spectrum in terms of the exhaustion of sources rather than in terms of the GZK-effect, discussed in the previous section (see the histograms in Fig. 1), provides also a good description of the evolution of $\langle X_{\max}\rangle$ and RMS($X_{\max}$) with energy, as seen by Auger. This is demonstrated exemplarily in Fig. 3 for the archetypal model from Ref. [22]. Similar results are reported, e.g., in Refs. [35,16].

The mixture of light and intermediate/heavy primaries at the highest energies predicted by the maximum-energy models may also explain the low level of directional correlations to nearby AGN. Enhancements, presently foreseen by the Pierre Auger Collaboration will address this issue (see below). Moreover, improving the composition measurement in the ankle region will be the key also to discriminate between different models proposed to explain the transition from Galactic to EG CRs. This has been a prime motivation for the HEAT and TALE extensions of the Pierre Auger and TA Observatories, respectively [36,37]. Clearly, the importance of measuring the composition up to the highest energy cannot be overstated as it will be the key to answering the question about the origin of the GZK-like flux suppression and the transition from Galactic- to extragalactic cosmic rays discussed above.

4. Anisotropies

4.1. Data for anisotropy searches

Further important information about the nature and origin of UHECR is contained in the distribution of their arrival directions over the sky. Unlike energies or primary mass, the arrival directions of cosmic ray events are practically free from systematic errors.

Modern cosmic ray experiments are well suited for studying the UHECR anisotropies at angular scales from about a degree up to the largest scales corresponding to the whole sky. The bulk of the arrival directions of UHECR events – those measured by the ground arrays – have an angular resolution of about $\sim 1^\circ$ [38,39]. The angular resolution may be up to an order of magnitude better for selected events observed by the fluorescence detectors in the stereo or hybrid modes [2], but the number of such events is much smaller. Most of the anisotropy studies discussed in what follows concerns data from the ground arrays. At $E > 10^{19}$ eV, the total number of events accumulated to date exceeds 10^4.

The ground arrays of both Auger and TA are fully efficient at energies larger than $3 \cdot 10^{18}$ eV [40] and 10^{19} eV [39], respectively. Above the efficiency thresholds (and certainly above 10^{19} eV) the integrated exposures of both experiments are very close to the geometrical one [41]. This makes the anisotropy study at high energies straightforward. Possible (mild) deviations from the geometrical exposure have to be studied and taken into account at energies below the efficiency threshold. Together, Auger and TA cover the whole sky.

4.2. Are anisotropies expected?

Apart from the (unknown) distribution of sources over the sky, two main factors that determine the UHECR anisotropy are deflections in cosmic magnetic fields and attenuation due to the interactions with the radiation backgrounds.

The extragalactic magnetic fields are known quite poorly. From measurements of the Faraday rotations of extragalactic sources, they are usually assumed to have a magnitude not exceeding $\lesssim 10^{-9}$ G [42] and a correlation length up to ~ 1 Mpc. In such a field, a proton of 10^{20} eV would be deflected by $\lesssim 2^\circ$ over a distance of 50 Mpc. Small deflections in the extragalactic fields are supported by simulations [43] which indicate that the extragalactic fields are small everywhere, except in

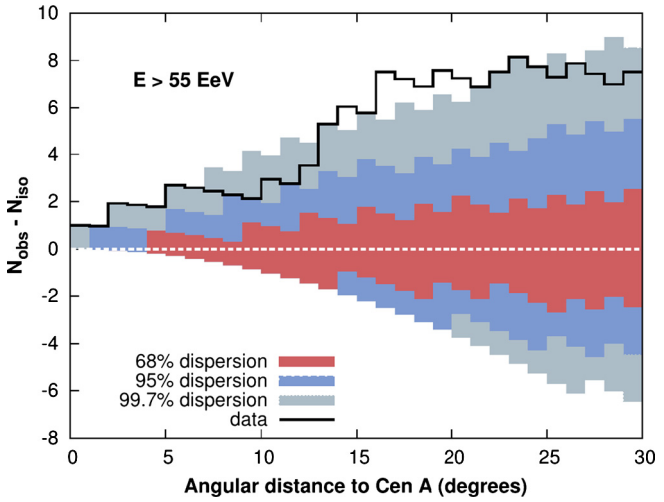

Fig. 4. Cumulative number of events with $E > 55$ EeV as a function of angular distance from the direction of Cen A [60]. The isotropic background is subtracted. The bands correspond to the dispersion expected for an isotropic flux.

galaxy clusters and filaments (see, however, [44] and further discussion in [45–47]). The arguments based on the analysis of the gamma-ray propagation [48,49] also point in this direction. An open, even though somewhat exotic, possibility is that the Milky Way itself is embedded in a filament with relatively strong magnetic fields, or that the Galactic wind has magnetized the space around our Galaxy [50,51].

The Galactic magnetic field is known much better. Models of its regular component have been constructed based on the existing measurements of the Faraday rotations of extragalactic sources [52,53]. This field would deflect a proton of 10^{20} eV by about 2–4° depending on the direction. The deflections in the random component of the Galactic field were argued to be subdominant [54,55].

Energy losses of UHECR become important at energies in excess of about $5 \cdot 10^{19}$ eV (GZK-effect [9,10]). Although the mass composition of UHECR is not known well, both protons and heavier nuclei are subject to a similar attenuation and have a propagation horizon of a few tens of Mpc at the highest energies.

As it is clear from the above numbers, if primary particles are predominantly protons, one might expect to recover the distribution of sources over the sky, with possibly bright spots of the size of a few degrees corresponding to individual bright sources. On the other hand, if primary particles are heavier nuclei, the flux distribution should be anisotropic in a manner similar (but not identical) to the source distribution at the scale of a few tens of degrees, but all the small-scale structure would be washed out. Note that because of the small propagation distance, at the highest energies the sources are expected to be distributed anisotropically due to the large-scale structure of the Universe.

None of these anisotropies is observed in the data. Below we summarize the tests that have been performed, and discuss possible implications of the results.

4.3. Searches for localized excesses of the UHECR flux

Two techniques are most commonly used to search for local excesses of the UHECR flux. One is based on the two-point angular correlation function (see, e.g., [56] for the realization of this method in the case of UHECR). This method is particularly useful in cases when there are no very bright spots but rather many excesses with a small amplitude and similar angular size. One then expects an excess in correlations at the corresponding angular scale. Both, Auger and TA data were examined in this way, so far with negative results [57,41].

Individual bright spots can be identified by looking for excesses in a moving window of given angular size and estimating the background either from Monte Carlo simulations or directly from the data. The overall significance should be corrected for the effective number of trials which is typically calculated by Monte Carlo simulations. The Pierre Auger collaboration has performed this kind of a blind search with window sizes of 5° and 15° in the data set with energy $E > 1$ EeV [18]. No significant excesses were found. In the TA data, analogous searches were performed in several energy bands around 1 EeV with a search window of 20° [58] and a position-dependent window of several degrees [59]. No significant deviation from isotropy was found.

At high energies (around and above the cutoff in the spectrum), the situation is more interesting. The Auger collaboration has reported an excess of the UHECR events with $E > 55$ EeV around the direction towards the Centaurus supercluster at a distance of about 60 Mpc and, towards Centaurus A, a close AGN at a distance of about 3.5 Mpc. The largest excess was found for a circular region of the angular size 18°. This region includes 10 out of 60 events above 55 EeV in the data set of this analysis, while 2.44 are expected from isotropy [60]. At lower energies, no excess was found. The cumulative number of

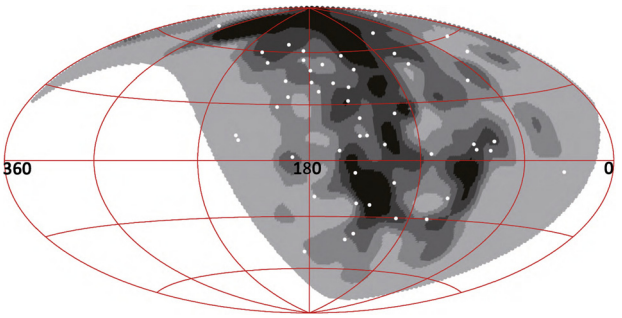

Fig. 5. The sky map of the TA events (white dots) with $E > 57$ EeV and the zenith angle cut $z < 55°$ in the Galactic coordinates. The bands of grey represent the expected UHECR flux assuming sources follow the matter distribution in the local Universe, smeared with the angular scale of 6°.

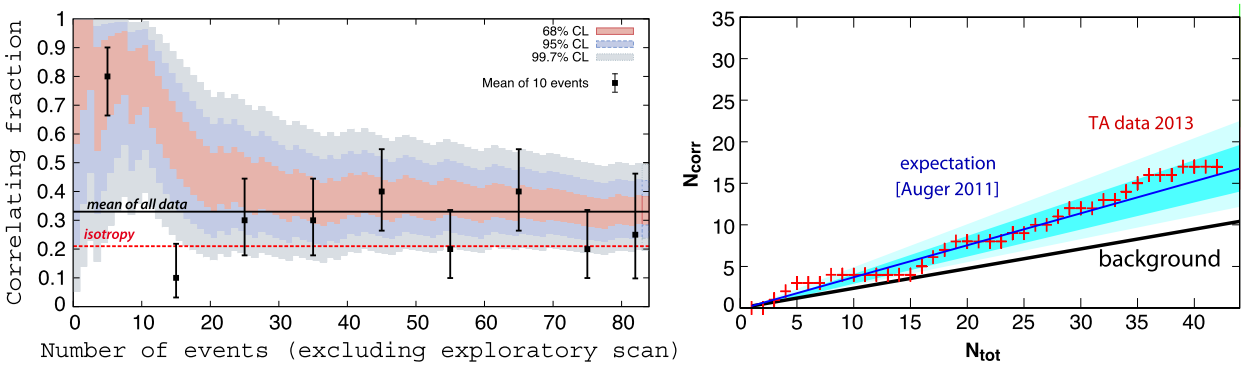

Fig. 6. Left: The most likely value of the degree of correlation $p_{\rm data} = k/N$ is plotted as a function of the total number of time-ordered events (excluding the data used for the parameter scan) [62]. The 68%, 95% and 99.7% confidence-level intervals around the most likely value are shaded. The horizontal red dashed line shows the isotropic value $p_{\rm iso} = 0.21$ and the full black line the current estimate of the signal $p_{\rm data} = 0.33 \pm 0.05$. The black symbols show the correlation fraction in independent bins with 10 consecutive events. Right: number of correlating events from TA (red crosses) [61] as a function of the total number of events. The black line shows the expected number of random coincidences assuming a uniform background. The latest data correspond to 17 correlating events out of 42. The shaded area shows the expectation (1- and 2σ bands) based on the degree of correlation measured by Auger [62]. (For interpretation of the references to color in this figure legend, the reader is referred to the web version of this article.)

events (with the background expectation subtracted) as a function of the angular distance from the direction of Centaurus A is shown in Fig. 4 together with 1-, 2- and 3σ bands representing fluctuations of the background.

In the Northern sky, the TA collaboration has also observed some deviation from isotropy in the data set with $E >$ 57 EeV at similar angular scales [61] in the direction about 20° from the Supergalactic plane, with no evident astrophysical structures in the closer vicinity. The corresponding sky map is shown in Fig. 5. The statistical significance of this "hot spot" has not been reported.

4.4. Search for point sources

If the UHECR composition is light and the deflections are dominated by the Galactic magnetic fields, or if the primary particles are neutral, one might expect that at the highest energies, arrival directions of UHECR events roughly point back to their sources. Because of the GZK cutoff, the UHECR propagation distance of trans-GZK events, i.e. events exceeding the GZK-threshold, is limited to 50–100 Mpc. The number of potential sources of UHECR in this volume is limited, and one may expect directional correlations between the position of candidate sources and the CR event directions. This kind of analysis is complementary to the one described above in the sense that it is optimized for the situation when none of the sources is sufficiently bright to produce a significant hot spot (cf. the discussion above).

The Auger collaboration has studied the correlation of the highest energy events above 55 EeV with the nearby Active Galactic Nuclei (AGNs) from the Véron–Cetty and Véron catalog (VCV) [63]. The parameters of the correlation (the energy threshold at 55 EeV, the maximum distance in the catalog of 75 Mpc and the maximum opening angle of 3.1°) were fixed from the exploratory scans in the independent data set [64,65]. The latest results of this study [62] is presented in Fig. 6 (left) which shows the most likely fraction of correlating events plotted as a function of the total number of events, together with the 1-, 2-, 3σ bands which allow one to see how far the observed number of correlated events deviates from the expectation assuming an isotropic background. One can see that while in the early part of the data there was a substantial deviation from isotropy, with the accumulation of events the correlation strength has decreased to $33 \pm 5\%$ compared to 21% expected from isotropy. The statistical significance for a departure from isotropy has over this period remained almost constant at a level between 2 and 3σ.

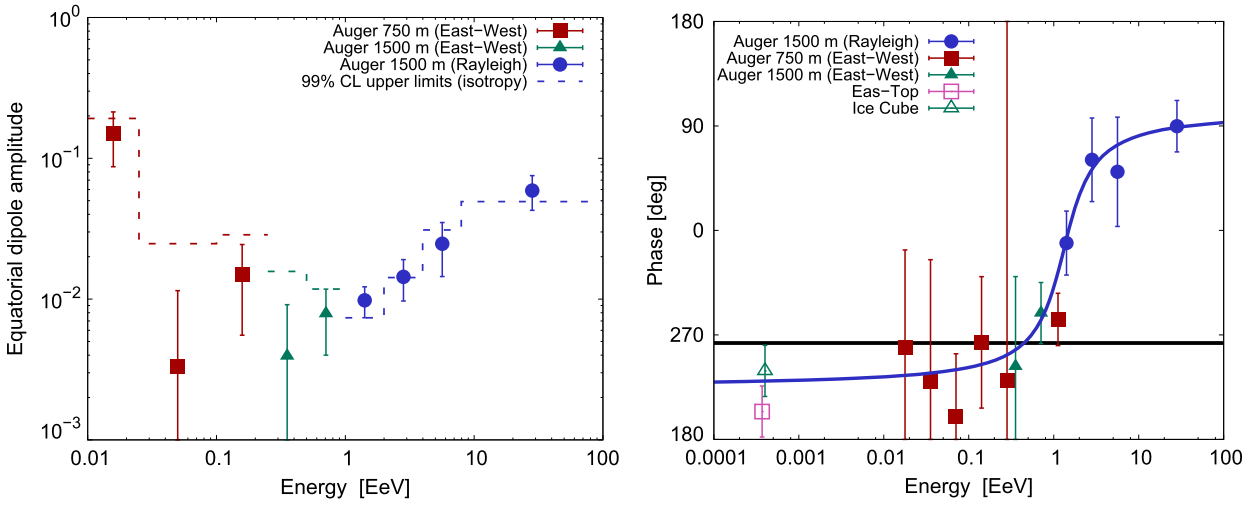

Fig. 7. *Left panel:* Equatorial dipole amplitude as a function of energy. The results of the modified Rayleigh analysis are shown with black circles and blue triangles corresponds to the analysis with East–West method. Red squares correspond to data from the infill array using the East–West method. The dashed lines are the 99% CL upper values of the amplitude that could result from fluctuations of an isotropic distribution. *Right panel:* Phase of the first harmonic as a function of energy. The horizontal black line corresponds to the value $\phi = 263°$, roughly coincident with the azimuthal direction to the Galactic center. The continuous blue curve is the fit to an empirical formula performed in [67]. (For interpretation of the references to color in this figure legend, the reader is referred to the web version of this article.)

Correlation with the same set of AGN and with the parameters fixed at the values set by the Auger collaboration analysis has been studied by the HiRes collaboration [66] with a negative result, and by the TA collaboration [41]. The most recent update of the TA analysis is presented in Fig. 6 (right), which shows the number of correlating events as a function of the total number of events. There is a slight excess of correlating events over the expected background, compatible with both the background and with the latest update on the AGN correlations from Auger. The expectation from the latest Auger data [62] is depicted by the 1- and 2σ bands, which demonstrates an excellent agreement of the two data sets. The combined probability to observe such a correlation from an isotropic distribution is below $p = 10^{-3}$, still too large to draw any firm conclusions.

4.5. Harmonic analysis

A standard tool in search for medium- and large-scale anisotropy searches is harmonic analysis. In the case of UHECR, the application of this method is limited by the incomplete sky coverage of presently existing observatories which cover either the southern (in the case of Auger) or northern (in the case of TA) part of the sky. For this reason, not all components of the low multipoles can be extracted unambiguously from the data of a single experiment. For instance, because of the (approximate) azimuthal symmetry of the exposure function, only the (xy)-components of the dipole (in equatorial coordinates) can be obtained in a straightforward way by a single experiment.

Results of a search for the equatorial dipole have been reported by the Pierre Auger collaboration [18,68]. Fig. 7 (left panel) shows the measurement of the dipole amplitude as a function of energy. Different analysis techniques have been used in different energy bins, as indicated in the plot. The measured amplitude of the dipole is consistent with expectations from the isotropic background. It is interesting to note, however, that the dipole amplitude is not the most sensitive observable [68] because of the energy binning and related loss in statistics. Even when the dipole amplitude is not sufficiently large to be detected, its phase may show regular behavior with energy, which would be an indication for a non-zero dipole. The right panel of Fig. 7 shows the phase of the dipole as a function of the energy. One can observe that the values of the phase are correlated in adjacent energy bins, and the phase behavior with energy is consistent with a continuous curve. This may indicate the presence of a non-zero dipole in the Auger data whose amplitude is just below the detection threshold.

The problem of the incomplete sky coverage may be resolved by combining the data of the two observatories. This is not a straightforward procedure because of the uncertainty in the relative flux calibration resulting mainly from possible differences in the energy scales of experiments. The difficulty, however, may be overcome, and the corresponding analysis is presently underway [69] with the first all-sky UHECR intensity presented at the ICRC 2013 with no significant under/over-densities found, yet [70].

4.6. Large-scale anisotropy

If the deflections of UHECR do not exceed 10–20°, as in the case of (predominantly) proton composition and small extragalactic magnetic fields, one should expect a correlation of UHECR arrival directions with the local large-scale structures (LSS). The largest correlations are expected at or above the GZK threshold energy, because in this energy range the

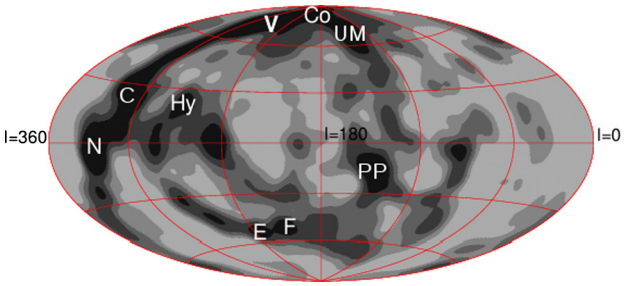

Fig. 8. Sky map of UHECR flux expected in a model where the sources follow the matter distribution, in Galactic coordinates. Darker regions correspond to larger flux. Each band integrates up to 1/5 of the total flux. Letters indicate nearby matter structures: C: Centaurus supercluster (60 Mpc); Co: Coma cluster (90 Mpc); E: Eridanus cluster (30 Mpc); F: Fornax cluster (20 Mpc); Hy: Hydra supercluster (50 Mpc); N: Norma supercluster (65 Mpc); PI: Pavo–Indus supercluster (70 Mpc); PP: Perseus–Pisces supercluster (70 Mpc); Ursa Major North group (20 Mpc) South group (20 Mpc); V: Virgo cluster (20 Mpc).

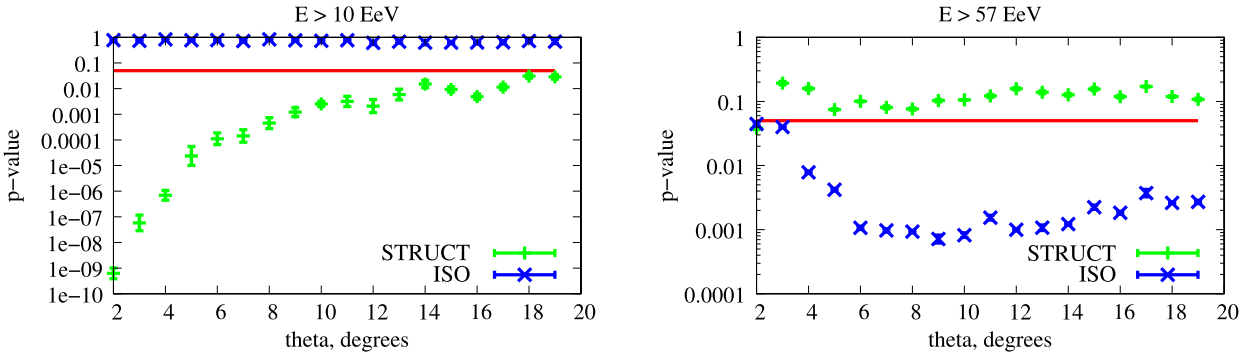

Fig. 9. The results of a statistical test for correlations between the LSS at different smearing angles θ and the TA data with $E > 10$ EeV (left panel) and $E > 57$ EeV. Green points represent p-values corresponding to the LSS model, blue points – to the isotropic distribution. (For interpretation of the references to color in this figure legend, the reader is referred to the web version of this article.)

propagation distance is limited to 50–100 Mpc and the contributions of the local structures are enhanced. With enough statistics, by checking such a correlation one may either discover it, or put a lower limit on the UHECR deflections. With some assumptions about cosmic magnetic fields, this information may also help to understand the UHECR composition.

The distribution of the UHECR flux expected in a generic model where sources trace the distribution of matter in the nearby Universe was calculated, e.g., in Ref. [71]. An improved version of this map obtained using a larger catalog of galaxies is presented in Fig. 8. This map was calculated assuming the UHECR are protons of energy 57 EeV, and smeared over an angular scale of 6°.

The expected flux map may be compared to the actual UHECR distribution by making use of an appropriate statistical test (see, e.g., [71]). The results of the analysis using the latest TA data set are shown in Fig. 9 for two datasets with $E > 10$ EeV and $E > 57$ EeV. One can see that at low energies ($E > 10$ EeV) the data are compatible with isotropy and incompatible with the LSS model for all but the largest smearing angles. At high energies, on the contrary, the data are compatible with the structure and not compatible with isotropy (the latter may be another manifestation of the "hot spot" discussed above).

A similar analysis has been performed using the first 69 publicly released Auger data [72] with energies $E > 55$ EeV. It was found that the correlation of the Auger events with the LSS prediction is larger than it would be in the isotropic model, but smaller than in the model where the UHECR sources follow the matter distribution in the Universe.

4.7. Other searches

If Galactic TeV gamma-rays originate from energetic protons suffering pion production interactions with ambient photons, protons, or nuclei, one should expect that neutrons are also produced. At energies higher than 10^{18} eV, neutrons can reach us from large parts of the Galaxy before they decay ($\tau_n = 9.2\ \text{kpc} \times E/\text{EeV}$). Since neutrons are not deflected by the magnetic fields, they should point back to their sources.

The Pierre Auger Collaboration has performed a dedicated search for Galactic sources of neutrons [73]. Several classes of sources were considered, such as H.E.S.S. TeV sources, several classes of pulsars, microquasars, and magnetars. These sources were stacked in their respective classes. The search window was set to the angular resolution of the detector. In addition to these sources, the Galactic plane and the Galactic Center were considered as possible sources. The advantage of this analysis over blind search is that the penalty for trials is substantially reduced. No statistically significant excess was detected in any of the catalogs, including the Galactic plane and the Galactic Center.

In a related analysis [74], a search for point sources of EeV photons was performed. With no photon point source being detected, upper limits on the photon flux have been derived for every direction within the Auger exposure map. None exceeds an energy flux of 0.25 $\mathrm{eV\,cm^{-2}\,s^{-1}}$ in any part of the sky, assuming a photon flux following $1/E^2$. These limits are of considerable astrophysical interest, because the energy flux in TeV gamma rays exceeds 1 $\mathrm{eV\,cm^{-2}\,s^{-1}}$ for some Galactic sources, with a differential spectral index of E^{-2} [75].

5. Conclusions and outlook

To summarize, the new generation of experiments – the Pierre Auger Observatory and the Telescope Array – have been constructed and operated in the last decade. Both experiments proved the advantage of the hybrid detector design where the fluorescence telescopes are combined with the ground array of detectors. The former are used for calorimetric energy measurements and calibration of the ground array energy scale, while the ground array takes advantage of its 100% duty cycle to accumulate large statistics. As a result, the uncertainty in the energy estimate has been reduced to much below 20%, and more than 10-fold increase in statistics has been achieved.

This has led to a number of important advances. First, the features in the UHECR energy spectrum – the ankle and the suppression at the highest energies – have been established beyond doubt. The spectral slopes before and after the ankle have been measured to the second digit and agree between the two experiments. The positions of the ankle also agree within the quoted errors, and are compatible with the existing model(s). The parameters of the break at the highest energies are known less accurately. There seems to be some discrepancy concerning the shape of the spectrum around the break; however more statistics is needed for a firm conclusion. The position of the break is compatible with the GZK cutoff for protons, but other explanations are also possible.

The substantial increase in statistics allowed one to put stringent constraints on the previously claimed deviations of the arrival directions from the isotropic distribution. This concerns the clustering of the UHECR events, as well as their correlations with different classes of putative sources. Unfortunately, no significant deviation from isotropy has been confirmed yet.

As far as the mass composition of UHECR is concerned, the situation is less definite, and a consistent picture has not yet emerged. While the Pierre Auger Observatory sees a change in the composition towards a heavier one at the highest energies, the TA observes no such a trend and is compatible with a pure proton composition. This difference in the data has profound consequences: the Auger data suggest that we see the maximum energy of sources, similarly to what is observed at the knee in the cosmic ray spectrum, while the TA data suggest we observe the GZK effect. Seeing the GZK effect would naturally allow us to interpret the ankle in terms of e^+e^--pair production losses in the CMB, while the maximum energy scenario relates the ankle to the transition from Galactic to extragalactic cosmic rays. The hard injection spectra required by the maximum energy model would either call for non-standard acceleration processes or require a contribution of nearby sources to the all-particle flux. Moreover, the different compositions in the GZK- and maximum-energy scenario will affect the level of anisotropies expected to be seen in the data. As already mentioned, a pure proton composition up to the highest energies starts to conflict with the highly isotropic UHECR sky, unless extremely strong Galactic and extragalactic magnetics fields are assumed.

Thus, despite the major advances, a number of key questions remain open: (i) a more accurate absolute energy calibration is needed to clarify the physical interpretation of the ankle and the high-energy break in the spectrum; (ii) the apparent differences in the observed mass composition at highest energies need to be understood; a more accurate modeling of air showers may be required for that in addition to a better understanding of systematic biases; (iii) the apparent absence of anisotropies, especially at the highest energies, has to be reconciled with the mass composition and our knowledge of the cosmic magnetic fields and the existing source models.

An important lesson from the existing picture is that the above open problems are closely interrelated. It is not inconceivable that a breakthrough in one of these questions will lead to the understanding of the others and finally to the emergence of a consistent picture of UHECR. The next advance in the experimental techniques, presently prepared by both collaborations, is therefore likely to be the last crucial step in our understanding of the nature and origin of these highest-energy particles ever observed in Nature.

Acknowledgements

We gratefully acknowledge stimulating discussions with out colleagues in the TA and Pierre Auger Collaborations. KHK acknowledges financial support by the German Ministry of Research and Education (Grants 05A11PX1 and 05A11PXA) and by the Helmholtz Alliance for Astroparticle Physics (HAP). PT acknowledges the support of the IISN project No. 4.4502.13, the RFBR grant 13-02-12175-ofi-m and Belgian Science Policy under IUAP VII/37.

References

[1] Pierre Auger Collaboration, J. Abraham, et al., Nucl. Instrum. Methods A 523 (2004) 50.
[2] Pierre Auger Collaboration, J.A. Abraham, et al., Nucl. Instrum. Methods A 620 (2010) 227, arXiv:0907.4282.
[3] TA Collaboration, Abu-Zayyad, et al., Nucl. Instrum. Methods A 689 (2012) 87, arXiv:1201.4964.
[4] TA Collaboration, H. Tokuno, et al., Nucl. Instrum. Methods A 676 (2012) 54, arXiv:1201.0002.

[5] KASCADE-Grande Collaboration, W. Apel, et al., Phys. Rev. Lett. 107 (2011) 171104, arXiv:1107.5885.
[6] KASCADE-Grande Collaboration, W.D. Apel, et al., Phys. Rev. D 87 (2013) 081101, arXiv:1304.7114.
[7] R. Aloisio, V. Berezinsky, A. Gazizov, Astropart. Phys. 39–40 (2012) 129, arXiv:1211.0494.
[8] V. Ptuskin, et al., Astron. Astrophys. 268 (1993) 726.
[9] K. Greisen, Phys. Rev. Lett. 16 (1966) 748.
[10] G.T. Zatsepin, V.A. Kuzmin, Pis'ma Zh. Eksp. Teor. Fiz. 4 (1966) 114.
[11] HiRes Collaboration, R.U. Abbasi, et al., Phys. Rev. Lett. 100 (2008) 101101, arXiv:astro-ph/0703099.
[12] Pierre Auger Collaboration, J. Abraham, et al., Phys. Rev. Lett. 101 (2008) 061101, arXiv:0806.4302.
[13] Pierre Auger, Telescope Array, Yakutsk Collaborations, B.R. Dawson, et al., EPJ Web Conf. 53 (2013) 01005, arXiv:1306.6138.
[14] TA Collaboration, E. Kido, O. Kalashev, arXiv:1310.6093, 2013.
[15] Pierre Auger Collaboration, A. Aab, et al., arXiv:1310.4620, 2013.
[16] R. Aloisio, V. Berezinsky, P. Blasi, arXiv:1312.7459, 2013.
[17] AIRFLY Collaboration, M. Ave, et al., Astropart. Phys. 42 (2013) 90, arXiv:1210.6734.
[18] Pierre Auger Collaboration, A. Aab, et al., arXiv:1307.5059, 2013.
[19] R. Aloisio, V. Berezinsky, A. Gazizov, Astropart. Phys. 34 (2011) 620, arXiv:0907.5194.
[20] D. Allard, Astropart. Phys. 39–40 (2012) 33, arXiv:1111.3290.
[21] P.L. Biermann, V. de Souza, Astrophys. J. 746 (2012) 72, arXiv:1106.0625.
[22] A.M. Taylor, Astropart. Phys. 54 (2014) 48, arXiv:1401.0199.
[23] K.-H. Kampert, et al., Astropart. Phys. 42 (2013) 41, arXiv:1206.3132.
[24] T.K. Gaisser, T. Stanev, S. Tilav, Front. Phys. China 8 (2013) 748, arXiv:1303.3565.
[25] S. Mollerach, E. Roulet, J. Cosmol. Astropart. Phys. 1310 (2013) 013, arXiv:1305.6519.
[26] K.-H. Kampert, M. Unger, Astropart. Phys. 35 (2012) 660, arXiv:1201.0018.
[27] R. Engel, D. Heck, T. Pierog, Annu. Rev. Nucl. Part. Sci. 61 (2011) 467.
[28] D. d'Enterria, R. Engel, T. Pierog, S. Ostapchenko, K. Werner, Astropart. Phys. 35 (2011) 98, arXiv:1101.5596.
[29] Pierre Auger Collaboration, P. Abreu, et al., Phys. Rev. Lett. 109 (2012) 062002, arXiv:1208.1520.
[30] TA Collaboration, H. Sagawa, et al. Highlight talk given at the 33rd Int. Cosmic Ray Conf., Rio de Janeiro, Brazil, 2013.
[31] Pierre Auger, TA, and Yakutsk-Collaborations, E. Barcikowski, et al., EPJ Web Conf. 53 (2013) 01006, arXiv:1306.4430.
[32] Pierre Auger Collaboration, J. Abraham, et al., Phys. Rev. Lett. 104 (2010) 091101, arXiv:1002.0699.
[33] W. Hanlon, et al., in: Proc. of the 33rd Int. Cosmic Ray Conf., Rio de Janeiro, Brazil, 2013, #0964.
[34] Pierre Auger, P. Abreu, et al., J. Cosmol. Astropart. Phys. 1302 (2013) 026, arXiv:1301.6637.
[35] D. Hooper, A.M. Taylor, Astropart. Phys. 33 (2010) 151, arXiv:0910.1842.
[36] Pierre Auger Collaboration, H. Mathes, et al., in: Proc. of the 32rd Int. Cosmic Ray Conf., vol. 3, Beijing, China, 2011, p. 149, arXiv:1107.4807.
[37] TA Collaboration, G. Thomson, et al., in: Proc. of the 32rd Int. Cosmic Ray Conf., vol. 3, Beijing, China, 2011, p. 331.
[38] Pierre Auger Collaboration, C. Bonifazi, et al., Nucl. Phys. Proc. Suppl. 190 (2009) 20, arXiv:0901.3138.
[39] TA Collaboration, T. Abu-Zayyad, et al., Astrophys. J. 768 (2013) L1, arXiv:1205.5067.
[40] Pierre Auger Collaboration, J. Abraham, et al., Nucl. Instrum. Methods A 613 (2010) 29.
[41] TA Collaboration, T. Abu-Zayyad, et al., Astrophys. J. 757 (2012) 26, arXiv:1205.5984.
[42] P.P. Kronberg, Rep. Prog. Phys. 57 (1994) 325.
[43] K. Dolag, D. Grasso, V. Springel, I. Tkachev, J. Cosmol. Astropart. Phys. 0501 (2005) 009, arXiv:astro-ph/0410419.
[44] G. Sigl, F. Miniati, T.A. Ensslin, Phys. Rev. D 70 (2004) 043007, arXiv:astro-ph/0401084.
[45] D. Ryu, H. Kang, J. Cho, S. Das, Science 320 (2008) 909, arXiv:0805.2466 [astro-ph].
[46] S. Das, H. Kang, D. Ryu, J. Cho, Astrophys. J. 682 (2008) 29, arXiv:0801.0371.
[47] D. Ryu, S. Das, H. Kang, Astrophys. J. 710 (2010) 1422.
[48] W. Essey, S. Ando, A. Kusenko, Astropart. Phys. 35 (2011) 135.
[49] F. Aharonian, W. Essey, A. Kusenko, A. Prosekin, Phys. Rev. D 87 (2013) 063002.
[50] E.-J. Ahn, G.A. Medina-Tanco, P.L. Biermann, T. Stanev, arXiv:astro-ph/9911123, 1999.
[51] J.E. Everett, E.G. Zweibel, R.A. Benjamin, D. McCammon, L. Rocks, J.S. Gallagher III, Astrophys. J. 674 (2008) 258.
[52] M. Pshirkov, P. Tinyakov, P. Kronberg, K. Newton-McGee, Astrophys. J. 738 (2011) 192, arXiv:1103.0814.
[53] R. Jansson, G.R. Farrar, Astrophys. J. 761 (2012) L11, arXiv:1210.7820.
[54] P.G. Tinyakov, I.I. Tkachev, Astropart. Phys. 24 (2005) 32, arXiv:astro-ph/0411669.
[55] M. Pshirkov, P. Tinyakov, F. Urban, arXiv:1304.3217, 2013.
[56] P.G. Tinyakov, I.I. Tkachev, JETP Lett. 74 (2001) 1, arXiv:astro-ph/0102101.
[57] Pierre Auger Collaboration, P. Abreu, et al., J. Cosmol. Astropart. Phys. 1204 (2012) 040.
[58] TA Collaboration, K. Kawata, et al., in: Proc. of the 33rd Int. Cosmic Ray Conf., Rio de Janeiro, Brazil, 2013, #0311.
[59] TA Collaboration, K. Kawata, et al., in: Proc. of the 33rd Int. Cosmic Ray Conf., Rio de Janeiro, Brazil, 2013, #0310.
[60] Pierre Auger Collaboration, P. Abreu, et al., J. Cosmol. Astropart. Phys. 1106 (2011) 022, arXiv:1106.3048.
[61] TA Collaboration, P. Tinyakov, et al., in: Proc. of the 33rd Int. Cosmic Ray Conf., Rio de Janeiro, Brazil, 2013, #1033.
[62] Pierre Auger Collaboration, K.-H. Kampert, arXiv:1207.4823, 2012.
[63] M. Veron-Cetty, P. Veron, Astron. Astrophys. 455 (2006) 773.
[64] Pierre Auger Collaboration, J. Abraham, et al., Science 318 (2007) 938, arXiv:0711.2256 [astro-ph].
[65] Pierre Auger Collaboration, P. Abreu, et al., Astropart. Phys. 34 (2010) 314, arXiv:1009.1855.
[66] HiRes Collaboration, R.U. Abbasi, et al., Astropart. Phys. 30 (2008) 175, arXiv:0804.0382.
[67] Pierre Auger Collaboration, P. Abreu, et al., Astropart. Phys. 34 (2011) 627, arXiv:1103.2721.
[68] Pierre Auger Collaboration, P. Abreu, et al., Astrophys. J. 762 (2013) L13, arXiv:1212.3083.
[69] Pierre Auger and TA Collaborations, P. Aab, et al., Searches for Large Scale Anisotropy in the Arrival Directions of Cosmic Rays Detected above 10^{19} eV at the Pierre Auger Observatory and the Telescope Array, 2014.
[70] TA and Auger Collaborations, A. Aab, et al., arXiv:1310.0647, 2013.
[71] H.B. Koers, P. Tinyakov, J. Cosmol. Astropart. Phys. 0904 (2009) 003, arXiv:0812.0860.
[72] F. Oikonomou, et al., J. Cosmol. Astropart. Phys. 1305 (2013) 015, arXiv:1207.4043.
[73] Pierre Auger Collaboration, P. Abreu, et al., Astrophys. J. 760 (2012) 148, arXiv:1211.4901.
[74] Pierre Auger Collaboration, D. Kuempel, et al., in: Proc. of the 33rd Int. Cosmic Ray Conf., Rio de Janeiro, Brazil, 2013, arXiv:1307.5059.
[75] J.A. Hinton, W. Hofmann, Annu. Rev. Astron. Astrophys. 47 (2009) 523.